Gas phase vibrational spectroscopy of cold $(TiO_2)_n^-$ (n = 3–8) clusters

Marissa L. Weichman,[1] Xiaowei Song,[2] Matias R. Fagiani,[2,3] Sreekanta Debnath,[2,3] Sandy Gewinner,[2] Wieland Schöllkopf,[2] Daniel M. Neumark,[1,4,a)] and Knut R. Asmis[3,a)]
[1]*Department of Chemistry, University of California, Berkeley, California 94720, USA*
[2]*Fritz-Haber-Institut der Max-Plank-Gesellschaft, Faradayweg 4-6, D-14195 Berlin, Germany*
[3]*Wilhelm-Ostwald-Institut für Physikalische und Theoretische Chemie, Universität Leipzig, Linnéstrasse 2, D-04103 Leipzig, Germany*
[4]*Chemical Sciences Division, Lawrence Berkeley National Laboratory, Berkeley, California 94720, USA*

(Received 17 December 2015; accepted 28 January 2016; published online 28 March 2016)

We report infrared photodissociation (IRPD) spectra for the D_2-tagged titanium oxide cluster anions $(TiO_2)_n^-$ with n = 3–8 in the spectral region from 450 to 1200 cm^{-1}. The IRPD spectra are interpreted with the aid of harmonic spectra from BP86/6-311+G* density functional theory calculations of energetically low-lying isomers. We conclusively assign the IRPD spectra of the n = 3 and n = 6 clusters to global minimum energy structures with C_s and C_2 symmetry, respectively. The vibrational spectra of the n = 4 and n = 7 clusters can be attributed to contributions of at most two low-lying structures. While our calculations indicate that the n = 5 and n = 8 clusters have many more low-lying isomers than the other clusters, the dominant contributions to their spectra can be assigned to the lowest energy structures. Through comparison between the calculated and experimental spectra, we can draw conclusions about the size-dependent evolution of the properties of $(TiO_2)_n^-$ clusters, and on their potential utility as model systems for catalysis on a bulk TiO_2 surface. © *2016 AIP Publishing LLC.* [http://dx.doi.org/10.1063/1.4942194]

INTRODUCTION

TiO_2 is an important, extensively studied semiconducting material, with varied applications as a catalyst, photocatalyst, catalyst support, gas sensor, and pigment.[1–4] TiO_2 was first identified as a photocatalyst for water splitting by Fujishima and Honda in 1972.[5] Since then its photoelectrochemical properties have been studied not only for further applications in water splitting catalysis[6,7] but also for use in photovoltaics,[8,9] the degradation of organic pollutants,[10,11] and CO_2 reduction.[12,13] In the bulk, TiO_2 exists in rutile, anatase, and brookite crystal structures;[2] the bulk rutile structure is the thermodynamic ground state under ambient conditions, but anatase is predicted to be the stable phase for nanoparticles smaller than 14 nm.[14]

An optimal photocatalyst should have a band gap tuned for absorption of the solar spectrum. The band gap of TiO_2, 3.05 eV for rutile and 3.15 eV for anatase,[15] allows for absorption of only ~5% of sunlight.[16] The use of TiO_2 nanostructures, perhaps in combination with doping, promises more tunable electronic structure for optimization of photocatalytic properties[17,18] and increased surface area for reaction. As such, various TiO_2 nanostructures have been synthesized and tested for wide applications.[19–24] Characterization of the properties of TiO_2 on the nano-scale is therefore of great interest.

Small gas-phase clusters are an insightful window into the study of larger metal oxide systems. In addition to being tractable for both experimental and computational studies, small clusters can serve as models for catalytically active point defect sites on surfaces,[25–27] which often demonstrate distinct bonding and stoichiometry from the bulk. Clusters display dramatically different structures and reactivity as a function of size;[28–30] their study can therefore elucidate the evolution of properties and emergence of macroscopic phenomena as one moves towards the bulk. Negatively charged $(TiO_2)_n^-$ clusters are particularly interesting models for catalysis, as photocatalytic reduction of CO_2 on bulk titania requires migration of a photoexcited electron to the surface and subsequent transfer to the adsorbate.[13] We therefore aim to characterize how the presence of an excess negative charge affects the structure and properties of titanium oxide clusters. In the current work, we use cryogenic ion trap vibrational spectroscopy of messenger-tagged, mass-selected anions to elucidate the structures of the $(TiO_2)_n^-$ clusters with n = 3–8.

Gas-phase titanium oxide clusters have been investigated with several experimental methods. Photoionization mass spectrometry experiments of neutral Ti_nO_m clusters generated with laser ablation showed that Ti_nO_{2n} and Ti_nO_{2n+1} stoichiometries were the most prevalent.[31] Infrared resonant multiphoton ionization experiments conducted on large neutral $(Ti_2O_3)_m(TiO_2)_n$ clusters compared the broad IR features observed to the phonon modes of bulk rutile TiO_2.[32,33] The IR multiple photon photodissociation (IRMPD) action spectrum of $Ti_4O_{10}^-$ has also been reported.[34,35] Anion photoelectron spectroscopy (PES) experiments on $(TiO_2)_n^-$ for n = 1–10[36,37] yielded the electron affinities and band gaps of the neutral clusters as a function of size, but lacking vibrational resolution could not shed light on cluster geometries. The reactivity of some small neutral and cationic titanium oxide clusters has also been studied experimentally with CO, CO_2, and small

a)Authors to whom correspondence should be addressed. Electronic addresses: dneumark@berkeley.edu and knut.asmis@uni-leipzig.de.

hydrocarbons.[38–41] Very recently, Yin and Bernstein[42] reported an experimental study of water oxidation on Ti_2O_4 and Ti_2O_5 neutral clusters under irradiation with visible light.

Higher-resolution spectroscopies have been applied to the smallest titanium dioxide clusters. The rotational, vibrational, and electronic structures of triatomic TiO_2 and TiO_2^- have been well studied.[43–46] IR spectra have been observed for neutral $(TiO_2)_2$ in a rare gas matrix.[47] A slow photoelectron velocity-map imaging study of cryogenically cooled anions (cryo-SEVI) identified the two lowest energy isomers of $(TiO_2)_2^-$ and elucidated the vibronic structure of the corresponding neutrals.[48]

While there is relatively little experimental work on $(TiO_2)_n$ with $n \geq 3$, a fair number of theoretical studies of neutral, and to a lesser extent, anionic clusters in this size range have been carried out. For the neutral clusters, most of the theoretical work has used density functional theory (DFT) to characterize the lowest-lying $(TiO_2)_n$ isomers in the range n = 1–15.[17,49–60] Only Qu and Kroes[51] and Tang *et al.*[58] report on low-lying anionic $(TiO_2)_n^-$ isomers with DFT. Several of these DFT studies made comprehensive searches for the global minimum energy neutral structures, using genetic algorithms,[50,60,61] simulated annealing,[50,61] systematic topological structure generation,[58] and basin hopping algorithms.[59] Of these studies, Tang *et al.*,[58] Marom *et al.*,[59] and Chen and Dixon[60] report the most thorough lists of candidate structures for neutral $(TiO_2)_n$ and are largely in agreement regarding the energetically lowest-lying isomers.

The highest-level theoretical results for $(TiO_2)_n$ and $(TiO_2)_n^-$ with n = 1–4 are reported by Li and Dixon,[18] using coupled cluster theory (CCSD(T)) with large basis sets, core-valence correlation, and scalar relativistic corrections. The predictions made in this coupled cluster study for the most stable $(TiO_2)_2^-$ isomers, as well as the same authors' analogous calculations for $(ZrO_2)_2^-$,[62] are in excellent agreement with recent high-resolution cryo-SEVI experiments.[48] Beyond the coupled-cluster study for n = 1–4,[18] the structures of the anionic $(TiO_2)_n^-$ clusters with $n \geq 5$ are not well-characterized theoretically, and the existing DFT reports are not in good agreement for many cluster sizes. The most stable anionic structures are also likely to differ from those of the corresponding neutral clusters.[18,48]

The combination of ion trapping and cooling with vibrational action spectroscopy[63] has emerged as a viable, sensitive method for structural characterization of complex gas-phase ions,[64,65] including mass-selected transition metal oxide cluster ions.[30,66] In this work, we present the first vibrationally resolved spectra of titanium dioxide cluster anions $(TiO_2)_n^-$ for n = 3–8, using infrared photodissociation (IRPD) spectroscopy. We also report a thorough DFT investigation of the energetics and vibrational structure of these anionic clusters. The experimental IR action spectra are acquired in the linear absorption regime via messenger-tagging of ions with D_2 in a radio frequency (RF) ion trap, and the measurement of D_2 loss upon irradiation with tunable IR light between 450 and 1200 cm^{-1}.[67] The positions and intensities of features in these IRPD spectra can be directly compared to simulated DFT results. The clusters are cooled in a clustering channel after production in a laser vaporization source and thermalized by many collisions with a cold buffer gas to cryogenic temperatures in the ion trap held at 14-25 K. In principle, this preparation ensures both that the clusters are vibrationally cold and that only the energetically most stable isomers are present.

Comparison of these IRPD spectra to calculations allows assignment of the most stable $(TiO_2)_n^-$ isomers for n = 3–8. We conclusively identify the C_s-symmetric lowest-lying isomer of $(TiO_2)_3^-$ and the C_2 lowest-lying $(TiO_2)_6^-$ structure and isolate the two low-lying structures that contribute to the experimental spectra of $(TiO_2)_4^-$ and $(TiO_2)_7^-$. The $(TiO_2)_5^-$ and $(TiO_2)_8^-$ clusters exhibit substantially more "glassy" potential energy surfaces, with many distinct, nearly energetically degenerate isomers. Nonetheless, the calculated spectra for the lowest energy isomers agree qualitatively with experiment, and we assign the dominant spectral contributions to these isomers. Through analysis of the calculated and experimental results for $(TiO_2)_n^-$ (n = 3-8), we can directly observe evolution of the properties of these titanium oxide clusters with size.

EXPERIMENTAL METHODS

The IRPD experiments in the present work were carried out with an ion trap tandem mass spectrometer[68,69] using tunable, intense IR radiation from the Fritz Haber Institute free electron laser (FHI FEL).[70] In brief, mass-selected $(TiO_2)_n^-$ clusters are cryo-cooled and messenger-tagged with D_2. The depletion of the messenger-tagged species after IR irradiation is monitored as a function of photon energy ($h\nu$),

$$(TiO_2)_n^- \cdot D_2 \xrightarrow{h\nu} (TiO_2)_n^{-*} \cdot D_2 \rightarrow (TiO_2)_n^- + D_2. \quad (1)$$

$(TiO_2)_n^-$ clusters are prepared in a pulsed laser vaporization source.[71] A frequency-doubled Nd:YAG laser operated at 50 Hz is focused onto a rotating titanium rod, and the resulting plasma is entrained in a pulse of 0.75% O_2 in He from a General Valve. Clusters are formed during subsequent expansion through a clustering channel. The ion beam then passes through a skimmer and into an RF decapole ion guide, filled with He to aid in collimation of the beam. The ions enter a quadrupole mass filter, which transmits only the desired $(^{48}Ti^{16}O_2)_n^-$ clusters. The beam is then deflected by 90° with an electrostatic quadrupole ion deflector and focused into an RF ring-electrode ion trap.[68] For the current work, the trap is filled continuously with a buffer gas consisting of either pure D_2 or a mixture of 10% D_2 in He and is held at cryogenic temperatures between 14 and 25 K. Ions are accumulated, thermalized, and messenger-tagged[67] through collisions with the buffer gas. For each $(TiO_2)_n^-$ cluster, the trap temperature and the composition of the buffer gas are optimized for tagging with a single D_2 molecule.

Ions are extracted from the trap at 5 Hz and are focused into the center of the extraction region of an orthogonal time-of-flight (TOF) mass spectrometer, where they are irradiated by a single macropulse from the FHI FEL. The TOF intensities of the tagged and bare ions are monitored as the FEL wavelength is scanned. The FHI FEL produces 210-3300 cm^{-1} radiation with a relative spectral bandwidth of ~0.5% fwhm.[70] Here we use the range 450–1200 cm^{-1} in 3 cm^{-1} steps; for

each step, ~100 TOF traces are acquired and averaged. Over this window, the FHI FEL has a spectral bandwidth ranging from 2 cm^{-1} fwhm at 450 cm^{-1} to 7 cm^{-1} fwhm at 1200 cm^{-1}, and a typical macropulse energy of 30-40 mJ. Attenuated laser pulses using 2%-33% of the full FEL power are employed to ensure operation within the linear absorption regime and avoid saturation. Different levels of attenuation may be required to observe all features linearly in the spectrum of a given species; spectral windows taken with different laser pulse energies are stitched together after processing.

The photodissociation cross section (σ_{IRPD})[71] can be calculated as a function of photon energy based on the relative abundance of the tagged parent ($I_P(\nu)$) and bare fragment ions ($I_F(\nu)$), the total ion signal, and the photon fluence $F(\nu)$,

$$\sigma_{IRPD} = -\ln\left[\frac{I_P(\nu)}{I_P(\nu)+I_F(\nu)}\right]/F(\nu). \quad (2)$$

CALCULATIONS

DFT calculations were carried out to find the relative energies, optimized geometries, harmonic vibrational frequencies, IR intensities, and vertical detachment energies of the lowest-lying $(TiO_2)_n^-$ isomers. We use the BP86 functional as it has been found to qualitatively reproduce higher-level CCSD(T) results for the energetics and geometries of metal oxide clusters[18,72] and has provided a good comparison for experimental spectroscopic work on TiO_2^- and $(TiO_2)_2^-$.[46,48] The 6-311+G* basis set was used for both Ti and O atoms, with full treatment of all electrons.[73,74] Transition state optimizations were also carried out with BP86/6-311+G* in order to locate isomerization barriers between $(TiO_2)_4^-$ clusters demonstrating similar bond connectivity. Additionally, we determined the harmonic vibrational frequencies for the lowest-lying $(TiO_2)_3^-$ cluster complexed with D_2. In this case, we use a semiempirical dispersion correction as parametrized by Grimme,[75] in addition to the BP86 functional, hereafter referred to as BP86+D. All *ab initio* calculations were carried out using Gaussian 09.[76]

Potential low-lying $(TiO_2)_n^-$ structures were identified through a comprehensive literature search. Chemical intuition alone is not sufficient to identify the most stable structural candidates, particularly for the larger clusters, owing to the complexity of the potential energy landscapes in question and the wealth of structural isomers. Thorough lists of low-lying anionic and neutral isomers have previously been identified by Li and Dixon[18] for n = 3-4 and Tang *et al.*[58] for n = 3-6, and by Marom *et al.*[59] for the neutral clusters with n = 3-10. We considered all reasonably low-lying structures proposed in these works and reoptimized them with spin-unrestricted BP86/6-311+G* calculations as doublet anions; the literature is in agreement that $(TiO_2)_n^-$ anions have a single unpaired electron.[18,48,51,58] All $\langle S^2\rangle$ values calculated for the clusters reported here fall very close to the expected value of 0.75 for doublet states. We report all $(TiO_2)_n^-$ (n = 3-8) isomers that were found to lie within 50 kJ/mol of the lowest energy structure after correction for vibrational zero point energies (ZPEs).

Full lists of calculated isomer energetics, electronic states, vertical detachment energies, harmonic vibrational frequencies above 400 cm^{-1}, and optimized geometries for all structures can be found in the supplementary material, as well as visualizations of the singly occupied molecular orbitals (SOMOs) of relevant clusters (Fig. S1).[81]

RESULTS AND DISCUSSION

Experimental IRPD spectra of the $(TiO_2)_n^-$ (n = 3-8) clusters in the region of 450–1200 cm^{-1} are shown in Fig. 1; the ion trapping temperatures used for each cluster are also indicated. Experimental peak positions and widths are reported in Table I. Structures, relative energies, point groups, and electronic states for all calculated low energy clusters are shown in Fig. 2. Simulated IR spectra for these isomers are plotted and compared to experimental results in Figs. 3–6. For ease of visual comparison, the experimental data in these figures are smoothed by averaging of adjacent data points from Fig. 1, reducing noise at the slight cost of resolution. Simulations are derived from unscaled harmonic vibrational frequencies and IR intensities and are plotted both as stick spectra (red) and as traces convoluted with a 10 cm^{-1} fwhm Gaussian line shape function (blue) to account for rotational band contours as well as the spectral width of the laser pulse.

Based on comparison of the IRPD results with the *ab initio* vibrational normal modes and harmonic spectra, $(TiO_2)_n^-$ clusters exhibit four general types of IR active vibrational modes, with characteristic frequency ranges delineated in

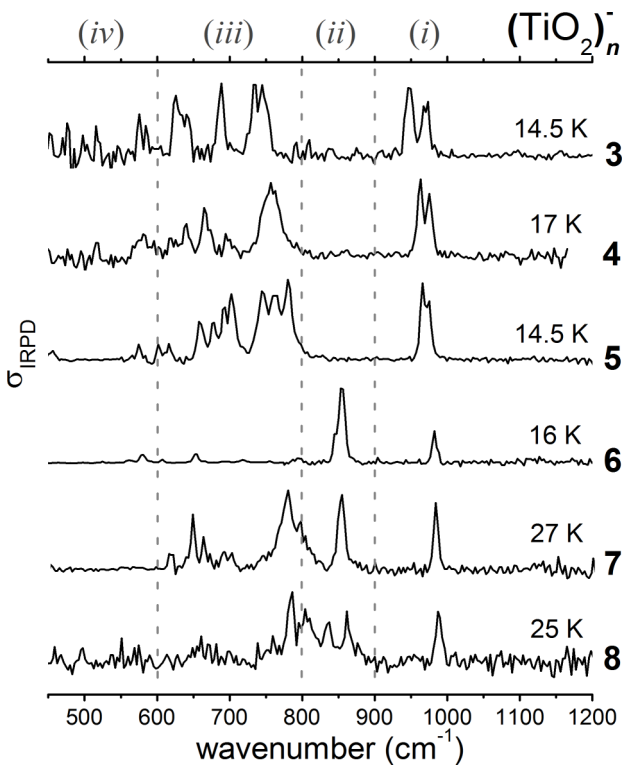

FIG. 1. Experimental IRPD spectra of D_2-tagged $(TiO_2)_n^-$ (n = 3-8) clusters. Regions (i)-(iv) of vibrational structure are marked with dashed lines. The trapping temperature for each cluster is also indicated.

TABLE I. Experimental vibrational frequencies (cm^{-1}) of $(TiO_2)_n^-$ clusters. Band positions and full widths at half-maximum (in parentheses) are determined by a least squares fit of a Gaussian line function to the experimental data.

Cluster	Region	Band positions (cm^{-1})
$(TiO_2)_3^-$	(i)	970(13), 948(15)
	(iii)	746(15), 733(8), 688(9), 640(12), 626(10)
	(iv)	576(6)
$(TiO_2)_4^-$	(i)	976(9), 963(9)
	(iii)	757(27), 697(12), 667(13), 640(9)
	(iv)	580(35), 517(8)
$(TiO_2)_5^-$	(i)	975(8), 966(7)
	(iii)	781(12), 763(15), 745(13), 703(13), 691(6), 678(11), 660(10), 616(11), 602(6)
	(iv)	575(6), 455(14)
$(TiO_2)_6^-$	(i)	982(8)
	(ii)	854(12)
	(iii)	794(15), 719(8), 653(8), 607(6)
	(iv)	580(8), 562(12)
$(TiO_2)_7^-$	(i)	982(7)
	(ii)	851(10)
	(iii)	795(11), 776(18), 700(6), 689(9), 661(6), 647(7), 616(7)
$(TiO_2)_8^-$	(i)	989(10)
	(ii)	862(6), 836(9), 806(20)
	(iii)	784(9), 760(4)

Fig. 1: (i) stretching modes of terminal Ti–O bonds (900-1000 cm^{-1}), (ii) stretching modes associated with groups of three Ti–O–Ti bridges tetrahedrally coordinated to a terminal Ti–O moiety (800-900 cm^{-1}), (iii) lower-frequency stretching modes of Ti–O–Ti bridges (600-800 cm^{-1}), and (iv) more delocalized bending, wagging, rocking, and ring breathing modes (<600 cm^{-1}). Qu and Kroes[51] have previously simulated IR absorption spectra for neutral $(TiO_2)_n$ (n = 2-9) clusters and noted similar categories of vibrational structure in these regions. Chen and Dixon[60] have also calculated terminal Ti–O stretching frequencies and IR intensities for the neutral clusters with n = 2-13.

In our experimental spectra, all six $(TiO_2)_n^-$ clusters with n = 3-8 show vibrational activity in region (i), indicating that each has dangling Ti–O bonds. Vibrational activity is seen in region (ii) for clusters with $n \geq 6$, while the smaller clusters show a distinctive gap with no absorption in this region. All clusters show structure in region (iii) with varying degrees of intensity, and most show weak structure in region (iv). Each experimental spectrum compares quite well qualitatively to the simulated spectrum of at least one low-lying predicted structure. The unscaled calculated frequencies of the best-fit simulations are generally lower than those observed experimentally, by factors of 0.99 in region (i), 0.97 in region (ii), and a range of 0.93-0.99 in regions (iii) and (iv).

We now give more detailed analysis of the experimental and theoretical results for each isomer in turn.

$(TiO_2)_3^-$

The experimental IRPD spectrum for $(TiO_2)_3^-$ (Fig. 3) exhibits an intense pair of vibrational features in region (i) along with a series of strong features spanning region (iii) and the high-frequency edge of region (iv). Comparison with DFT results supports an unambiguous assignment of the experimental spectrum to the isomer **3-1**, based on calculated energetics and simulated linear IR spectra.

The **3-1** C_s structure has been previously calculated to be the ground state structure for the n = 3 anion[18,51,58] and is widely agreed upon as the global minimum energy structure for the neutral n = 3 cluster as well.[17,18,49–61] The next lowest-lying anionic isomer, the C_2 structure **3-2**, is calculated to lie 92 kJ/mol higher in energy with BP86/6-311+G*; with CCSD(T), Li and Dixon[18] find that the **3-2** anion lies 172 kJ/mol above **3-1**. The presence of the **3-2** structure experimentally can be ruled out based on these energetics and the considerably poorer agreement between its simulated spectrum and experiment.

Through comparison with the simulated IR spectrum of isomer **3-1** in Fig. 3, we can assign the experimental vibrational features. The two highest-frequency vibrations observed here at 970 cm^{-1} and 948 cm^{-1} correspond respectively to symmetric and antisymmetric stretching modes involving the two terminal Ti–O bonds. At the BP86/6-311+G* level of theory, these modes are calculated to lie at 961 cm^{-1} and 938 cm^{-1}, respectively. The series of experimental peaks at 746 cm^{-1}, 733 cm^{-1}, 688 cm^{-1}, 640 cm^{-1}, 626 cm^{-1}, and 576 cm^{-1} are various stretching modes of Ti–O–Ti bridges in the central ring of the cluster. These features are well-matched by calculated frequencies of 724 cm^{-1}, 723 cm^{-1}, 665 cm^{-1}, 611 cm^{-1}, 605 cm^{-1}, and 554 cm^{-1}. The separation of the two highest energy modes (724/723 cm^{-1}) in region (iii) increases from 1 cm^{-1} to 6 cm^{-1} when the D_2 tag is considered explicitly in a BP86+D/6-311+G* calculation (see Fig. S2 in the supplementary material),[81] in improved agreement with the experimental observation of two maxima separated by 13 cm^{-1}. The experimental features in region (iii) show decreasing intensity with decreasing frequency; the calculated spectrum demonstrates qualitatively similar structure.

$(TiO_2)_4^-$

The experimental IRPD spectrum of $(TiO_2)_4^-$ (Fig. 3) shows an intense, narrowly spaced pair of peaks in region (i), one very intense, broad feature on the high energy side of region (iii), and several weaker features spanning regions (iii) and (iv).

There are three low-lying structures for $(TiO_2)_4^-$. The literature is in reasonable agreement that for the neutral cluster, the C_{2v} structure **4-2** yields the lowest energy.[17,18,50,52–54,56,58–61] Previous DFT studies by Qu and Kroes[51] and Tang *et al.*[58] concur with our BP86/6-311+G* results that the C_{2v} structure **4-1** gives the most stable anion. We find that in the anion, **4-2** and **4-3** lie 22 kJ/mol and 26 kJ/mol above **4-1**, respectively. CCSD(T) calculations by Li and Dixon[18] find the C_{2h} structure **4-3** lowest in energy for the anion, with **4-2** and **4-1** lying incrementally higher in energy

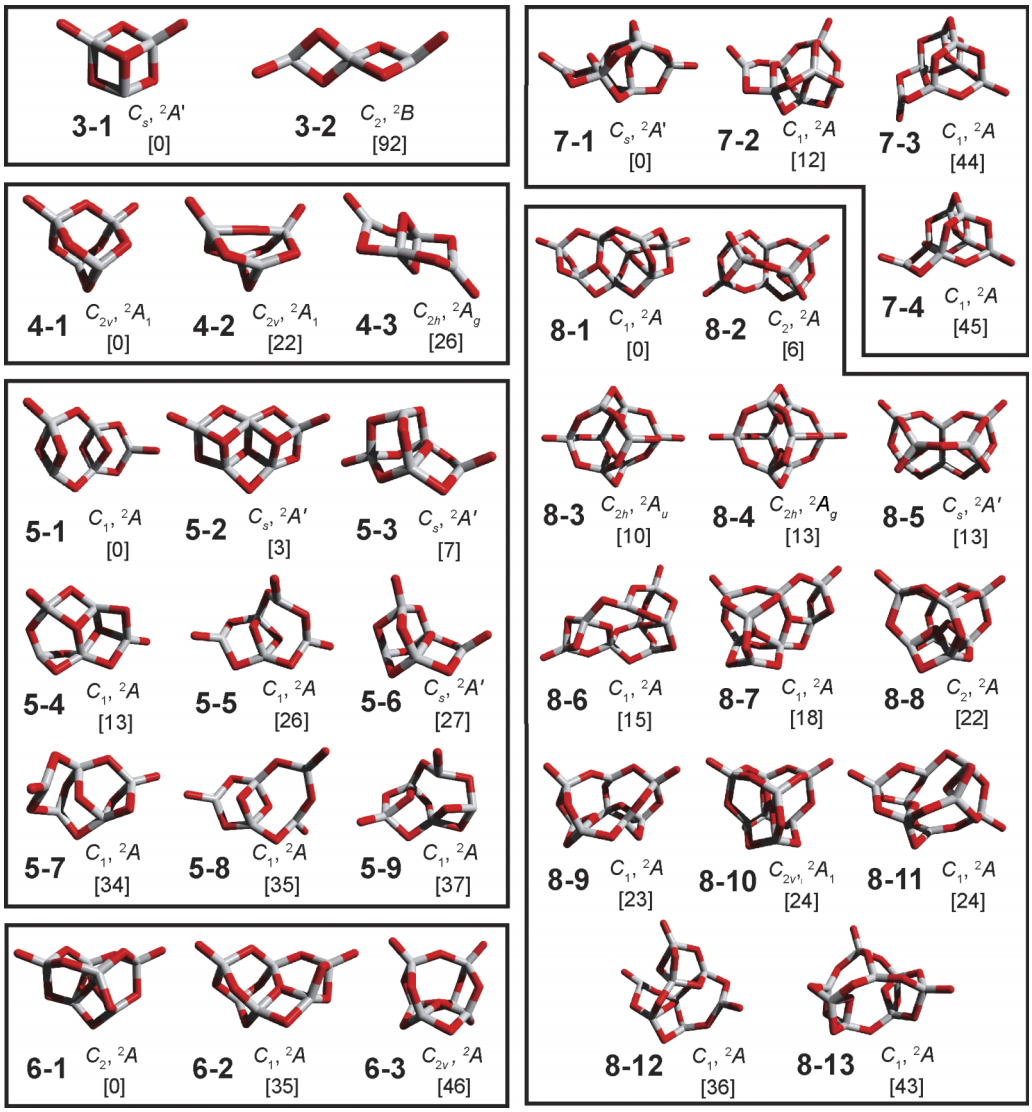

FIG. 2. BP86/6-311+G* minimum energy structures, point groups, electronic states, and relative energies (kJ/mol) of energetically low-lying isomers of $(TiO_2)_n^-$ (n = 3-8) clusters.

by 1 kJ/mol and 3 kJ/mol, respectively. The CCSD(T) results of Li and Dixon accurately predicted the energetic ordering of anionic isomers observed experimentally in photodetachment of $(TiO_2)_2^-$,[48] where DFT methods had failed.[51,58] The relative energies of the $(TiO_2)_4^-$ isomers given by CCSD(T) may therefore be more trustworthy than the DFT values, in which case the three $n = 4$ isomers are predicted to be nearly isoenergetic.

The experimental $n = 4$ spectrum has a strong feature in region (iii) at 757 cm^{-1}, and no structure in region (ii). The simulated spectrum of **4-1** (Fig. 3) has intense IR absorptions in region (ii) at 825 cm^{-1} and 822 cm^{-1}, corresponding to antisymmetric and symmetric Ti–O–Ti bridge stretching; analogous strongly IR active bridge-stretching modes are shifted to lower frequencies of 706 cm^{-1} and 696 cm^{-1} in **4-2**. The strong region (ii) modes of **4-1** have frequencies much higher than experiment, especially given the general trend that calculated frequencies for the best-fit isomers are consistently lower than experimental values. The corresponding IR active transitions in **4-2**, however, are predicted too low to provide a good match with experiment, at factors of 0.92-0.93 lower than the experimental value. It is, therefore, worth considering if the experiment probes a fluxional cluster encompassing the **4-1** and **4-2** basins, with vibrational frequencies that are not well represented by the harmonic approximation.

Unlike most clusters reported in this work, **4-1** and **4-2** have identical bond connectivity. With BP86/6-311+G*, the transition state between **4-1** and **4-2** is of C_s symmetry and lies 36 kJ/mol above **4-1** and only 14 kJ/mol above **4-2** without ZPE correction. By comparison, the barrier between structures **4-2** and **4-3** lies much higher in energy: 67 kJ/mol above **4-2** and 63 kJ/mol above **4-3**. Such a small **4-1**/**4-2** barrier suggests that these isomers are perhaps not separate spectroscopic species, but two shallow local minima of a rather floppy system. The *ab initio* harmonic frequency analysis of **4-1** and **4-2** therefore may not accurately capture the vibrational signature of this particular Ti–O–Ti bridging motif. For comparison, we plot the calculated IR spectrum of the **4-1**/**4-2** transition state alongside the **4-1** and **4-2** spectra in

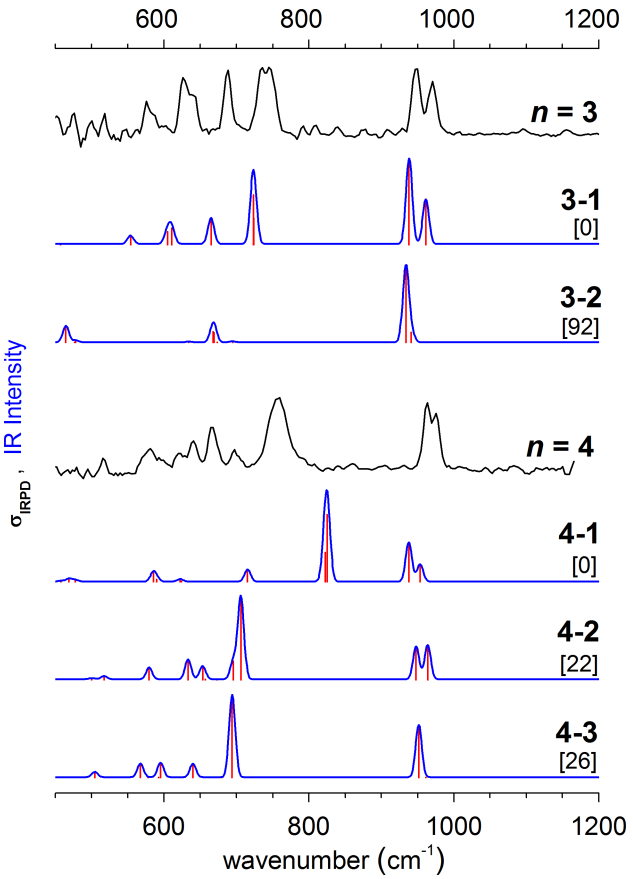

FIG. 3. Smoothed experimental IRPD spectra (black) of D_2-tagged $(TiO_2)_n^-$ ($n = 3, 4$) and simulated linear IR absorption traces (blue), stick spectra (red), and relative energies (kJ/mol) of the predicted lowest-lying isomers at the BP86/6-311+G* level of theory.

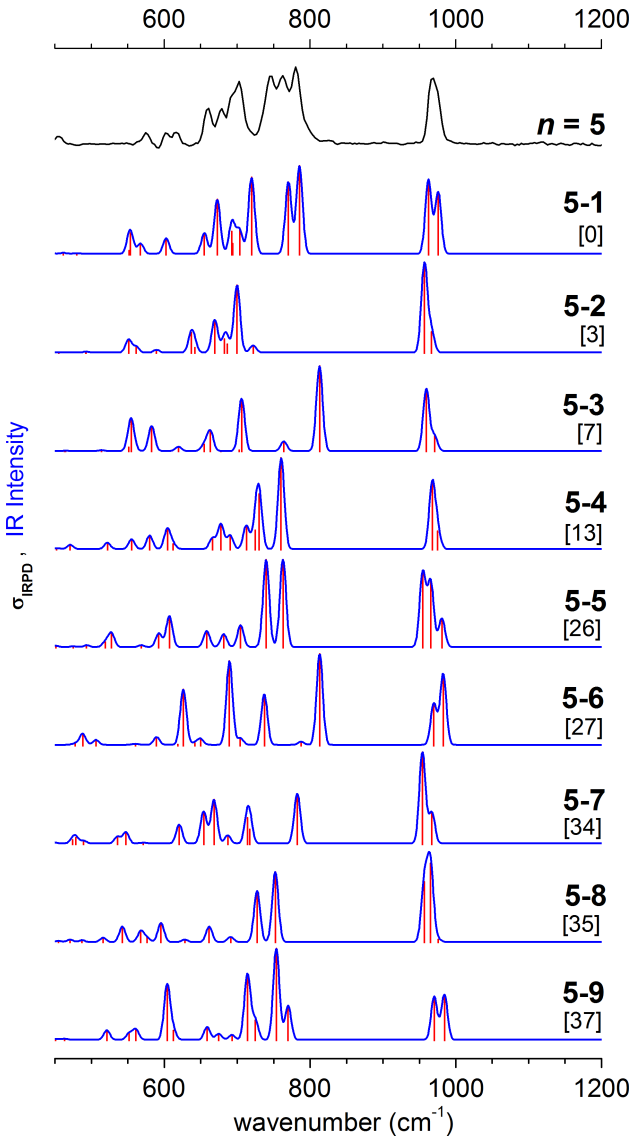

FIG. 4. Smoothed experimental IRPD spectrum (black) of D_2-tagged $(TiO_2)_n^-$ ($n = 5$) and simulated linear IR absorption traces (blue), stick spectra (red), and relative energies (kJ/mol) of the predicted lowest-lying isomers at the BP86/6-311+G* level of theory.

Fig. S3.[81] The **4-1**/**4-2** TS spectrum looks intermediate to those of the **4-1** and **4-2** isomers, lending further support to an assignment to a fluxional **4-1**/**4-2** system. Though beyond the scope of the current work, it would be of interest to investigate the isomerization barrier between these two structures at the CCSD(T) level of theory.

A significant contribution from isomer **4-3** is unlikely based on the vibrational structure in region (i). Experimentally, we observe peaks at 976 cm^{-1} and 963 cm^{-1} corresponding to two free Ti–O stretching modes. In structure **4-3**, based on the C_{2h} symmetry of the system, only the antisymmetric Ti–O stretching mode calculated at 952 cm^{-1} is IR active. The C_{2v} **4-1** and **4-2** structures, on the other hand, have two IR active modes in this region, at 953 cm^{-1} and 938 cm^{-1} for **4-1**, and 964 cm^{-1} and 948 cm^{-1} for **4-2**, and can therefore account for all features observed experimentally. We cannot, however, rule out a small contribution from isomer **4-3**. The calculated frequency of the IR active Ti–O stretching mode for **4-3** falls close to the two calculated frequencies for **4-1** and **4-2** and could contribute to the doublet feature observed in region (i).

$(TiO_2)_5^-$

The $(TiO_2)_5^-$ IRPD spectrum (Fig. 4) shows a single somewhat broad feature in region (i), a series of closely spaced, intense absorption features in region (iii), and weaker features extending into region (iv).

Nine $(TiO_2)_5^-$ isomers are calculated to lie within 50 kJ/mol of the lowest energy cluster, many of which are effectively degenerate within the accuracy of DFT. Our calculations find the C_1-symmetric **5-1** structure lowest in energy, with two C_s structures, **5-2** and **5-3**, lying 3 kJ/mol and 7 kJ/mol higher, respectively. Prior DFT work by Tang *et al.*[58] reports **5-2** as the anion global minimum energy structure, while Qu and Kroes[51] report **5-3** as the ground state. The neutral $n = 5$ cluster is also observed to have a "glassy" potential energy surface with many low-lying structures.[59] Most DFT studies in the literature report either **5-2** or **5-3** as the neutral global minimum energy structure,[50–54,56–61] with both structures often reported to lie within 3 kJ/mol of one another.[58–61]

Among the many calculated low-lying clusters, the simulated IR spectrum of structure **5-1** (Fig. 4) best reproduces

the observed experimental features, particularly the strong peaks between 700 and 800 cm^{-1}. Intense experimental peaks in the upper half of region (iii) at 781 cm^{-1}, 763 cm^{-1}, and 745 cm^{-1} reasonably match the strongly IR active modes for **5-1** at 785 cm^{-1}, 770 cm^{-1}, and 720 cm^{-1}. Structure **5-1** also exhibits two Ti–O stretching modes in region (i) at 976 cm^{-1} and 962 cm^{-1} that are resolved in the unsmoothed spectrum in Fig. 1 at 975 cm^{-1} and 966 cm^{-1}.

Other low-lying isomers may well contribute to the observed structure in the experimental spectrum. For instance, structure **5-2** could contribute to the absorption in region (i) and the lower frequency side of region (iii), but it cannot alone explain the observed experimental features, as it is lacking in intense structure between 700 and 800 cm^{-1}. Isomer **5-4** similarly may be involved with absorption in the higher frequency side of region (iii), but on its own does not have enough distinct IR active modes to match experiment. Structures **5-3** and **5-6** can be ruled out, as they predict absorption in region (ii) due to the presence of a free Ti–O moiety bound to three roughly tetrahedrally coordinated Ti–O–Ti bridges in both structures. Structure **5-5** can also most likely be ruled out, as it has three Ti–O dangling bonds, and thus three IR active modes in region (i) that should yield broader absorption than what is observed experimentally.

It is remarkable that given the plethora of low-lying calculated structures for $(TiO_2)_5^-$, the simulated IR spectrum of the lowest-lying DFT structure **5-1** is a qualitative match with experiment and may indicate a dominant contribution from this isomer. It is also possible that, as for $n = 4$, the $(TiO_2)_5^-$ anions demonstrate fluxional character, and that nearby local minima on the glassy $n = 5$ potential energy surface contribute to the IR spectrum in a way not captured by our harmonic IR simulations.

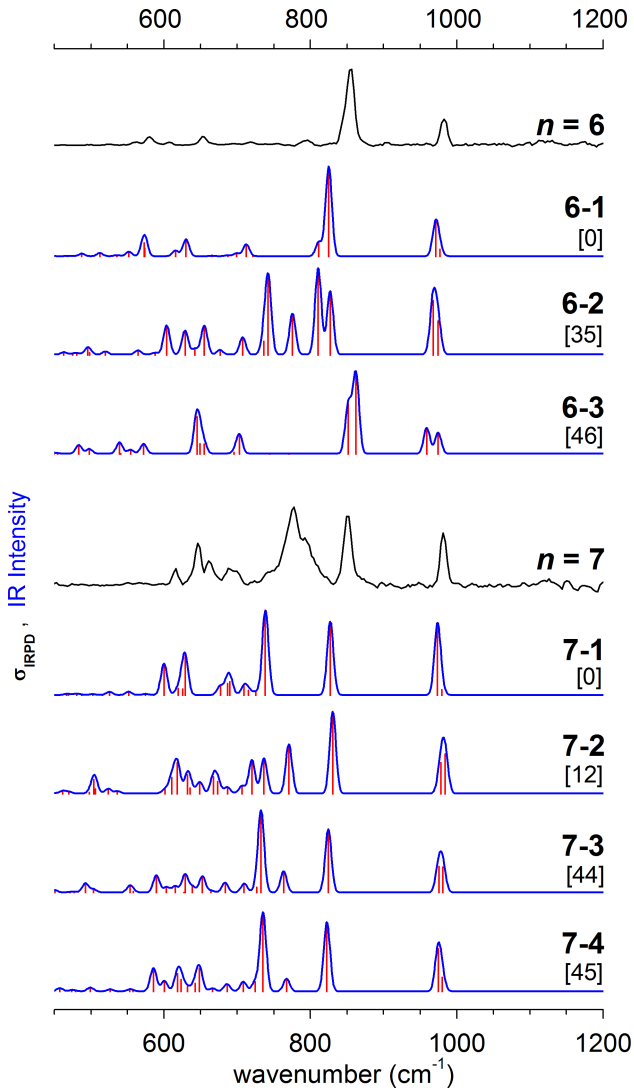

FIG. 5. Smoothed experimental IRPD spectra (black) of D_2-tagged $(TiO_2)_n^-$ ($n = 6, 7$) and simulated linear IR absorption traces (blue), stick spectra (red), and relative energies (kJ/mol) of the predicted lowest-lying isomers at the BP86/6-311+G* level of theory.

$(TiO_2)_6^-$

The IRPD spectrum for $(TiO_2)_6^-$ (Fig. 5) is distinct from that of the other clusters in its simplicity. The spectrum is dominated by a single very intense peak in region (ii) and shows a single weak feature in region (i) along with a handful of very weak features in regions (iii) and (iv). Using calculated energetics and simulated IR spectra, the experimental spectrum can be assigned unambiguously to the C_2-symmetric **6-1** isomer.

Prior DFT studies for the $n = 6$ anion by Qu and Kroes[51] and Tang *et al.*[58] have reported **6-1** as the most stable isomer; this structure has also been fairly widely identified as the lowest-lying neutral structure.[51,53,56,58–61] We identify two energetically higher-lying isomers, the C_1 structure **6-2** and the C_{2v} structure **6-3**, at 35 kJ/mol and 46 kJ/mol above **6-1**, respectively. **6-2** can be ruled out due to the poor match between the experimental and simulated spectra; **6-3** is a poorer match to the experimental spectrum than **6-1** and is calculated to lie at a high enough relative energy that it can be safely ruled out as well.

We can assign the observed vibrational features through comparison with the simulated IR spectrum of isomer **6-1** (Fig. 5). The peak observed in region (i) at 982 cm^{-1} corresponds largely to the antisymmetric Ti–O stretching mode, calculated at 971 cm^{-1}. The experimental feature in region (ii) appears at 854 cm^{-1} and is matched by a strongly IR active calculated mode at 825 cm^{-1}. This mode corresponds to antisymmetric umbrella-like stretching of the two groups of tetrahedrally coordinated Ti–O–Ti bridges connected to each free Ti–O moiety. Considering the much weaker features in regions (iii) and (iv), the observed peaks at 719 cm^{-1}, 653 cm^{-1}, and 580 cm^{-1} align with predicted weakly IR active Ti–O–Ti bridge stretching modes at 712 cm^{-1}, 630 cm^{-1}, and 573 cm^{-1}.

$(TiO_2)_7^-$

The IRPD spectrum for $(TiO_2)_7^-$ (Fig. 5) has a single sharp peak in region (i), a single peak in region (ii), a broad, strong peak at the high-frequency edge of region (iii), and weaker features extending through region (iii) towards lower frequencies.

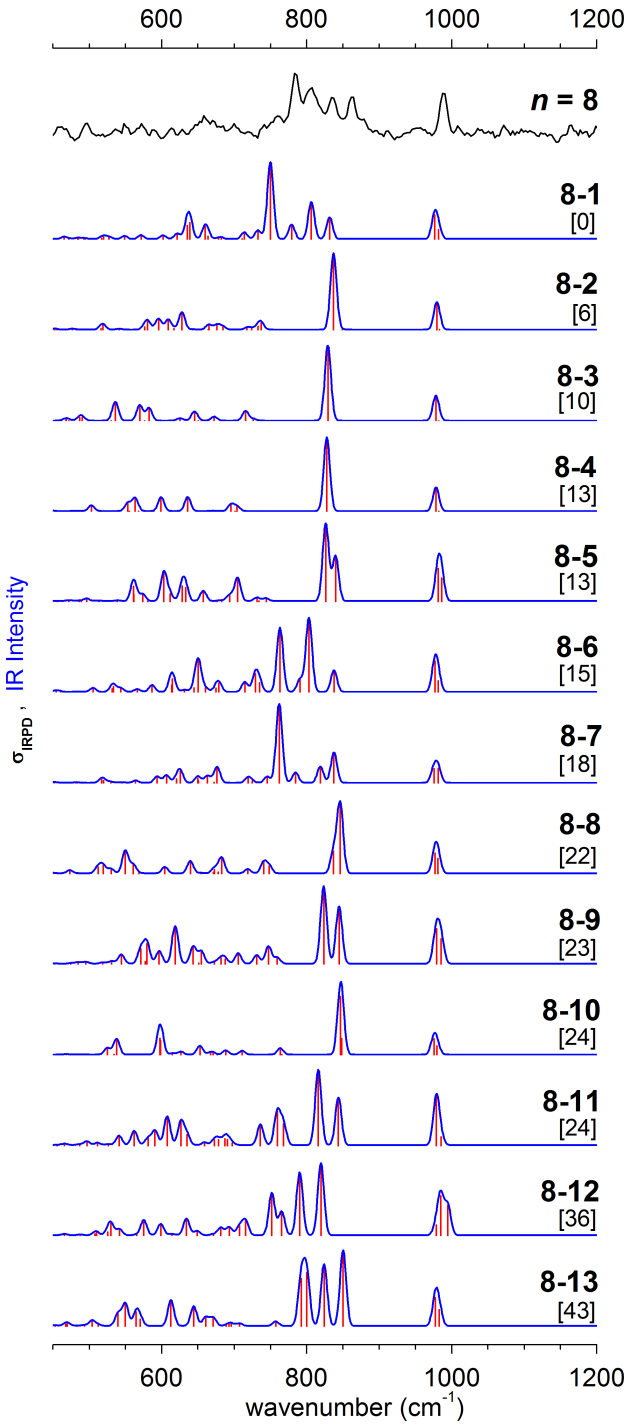

FIG. 6. Smoothed experimental IRPD spectrum (black) of D_2-tagged $(TiO_2)_n^-$ ($n = 8$) and simulated linear IR absorption traces (blue), stick spectra (red), and relative energies (kJ/mol) of the predicted lowest-lying isomers at the BP86/6-311+G* level of theory.

Four $n = 7$ isomers lie within 50 kJ/mol of the lowest energy structure. The C_s isomer **7-1** is the most stable, with the C_1-symmetric **7-2** structure lying 12 kJ/mol above, and additional C_1 isomers **7-3** and **7-4** lying 44 and 45 kJ/mol above. Beginning with $n = 7$, the literature becomes sparse regarding thorough reports for the most stable clusters. Only Qu and Kroes[51] have published DFT structures and energetics for anions with $n \geq 7$, but they did not perform a thorough structure search, and thus do not report the isomers we find to be the lowest in energy. Better searches exist for the global minimum structures of the neutral $(TiO_2)_n$ clusters. Structures **7-1** and **7-2** have been identified as the two lowest-lying neutral cluster isomers by Chelikowsky[59] and Dixon;[60] Chaudhury[61] also finds **7-1** to be the most stable neutral cluster.

All four $n = 7$ structures reported here have simulated IR spectra that compare reasonably well to experiment (Fig. 5). The experimental features at 982 cm^{-1} in region (i) and 851 cm^{-1} in region (ii) are reproduced by strongly IR active modes in all four isomers, at 974 cm^{-1} and 827 cm^{-1} for **7-1**, 984/978 cm^{-1} and 831 cm^{-1} for **7-2**, 981/975 cm^{-1} and 824 cm^{-1} for **7-3**, and 975 cm^{-1} and 822 cm^{-1} for **7-4**. The features in region (i) correspond to symmetric/antisymmetric free Ti–O stretches, while those in region (ii) involve stretching of the three tetrahedrally coordinated Ti–O–Ti bridges at the single Ti–O moiety with 4-fold coordination.

More distinctive is the broad, intense structure observed at the high frequency edge of region (iii) between 750 and 810 cm^{-1}. Within this broad feature lie an intense peak at 776 cm^{-1}, and a weaker shoulder at 795 cm^{-1}. This feature cannot be explained by the simulated IR spectrum of a single isomer; however, it could be modeled by the presence of both isomers **7-1** and **7-2**, or perhaps a fluxional cluster encompassing both structures. In particular, the strong absorptions of isomer **7-1** at 738 cm^{-1} and of isomer **7-2** at 771 cm^{-1} match well with the intense peak and shoulder of this broad feature, respectively, and additional IR active modes of **7-2** at 720 cm^{-1} and 736 cm^{-1} could also contribute intensity in this region. Isomers **7-3** and **7-4** could also contribute to the experimental spectrum but lie significantly higher in energy. We, therefore, assign the experimental spectrum to a combination, perhaps fluxional in nature, of isomers **7-1** and **7-2**.

$(TiO_2)_8^-$

The IRPD spectrum for $(TiO_2)_8^-$ (Fig. 6) has a single feature in region (i), a dense cluster of features between 770 and 880 cm^{-1} spanning region (ii) and the high frequency edge of region (iii), and weaker, unresolved features in the lower frequency span of region (iii).

$(TiO_2)_8^-$ has many isomers lying close in energy; with DFT we identify thirteen $n = 8$ anionic structures within 50 kJ/mol of the lowest energy structure. The most stable structure **8-1** is of C_1 symmetry and is quite disordered compared to the C_2, C_{2h}, and C_s structures **8-2** through **8-5** that lie only slightly higher in energy. The only theoretical study for anions with $n = 8$ is presented by Qu and Kroes,[51] who do not report the structures we identify as the lowest in energy, and again, considerably more work has been done to search for the lowest energy neutral structures. Marom *et al.*[59] report the most thorough list of neutral isomers found with basin hopping and note that like the $n = 5$ cluster, the $n = 8$ cluster also has a particularly "glassy" potential energy surface. Despite this, there is some agreement in the literature that the most stable neutral $n = 8$ cluster is a C_{2h} species analogous to the isomers **8-3** and **8-4** reported here.[53,56,59–61]

The experimental spectrum shows one peak in region (i) at 989 cm^{-1} and four peaks of increasing intensity in regions

(ii) and (iii) at 862 cm^{-1}, 836 cm^{-1}, 806 cm^{-1}, and 784 cm^{-1}, with a weaker shoulder at 760 cm^{-1}. The spectrum of the **8-1** isomer is a good match for the experimental data (Fig. 6), with calculated close-lying symmetric and antisymmetric Ti–O stretching modes at 982 cm^{-1} and 976 cm^{-1} in region (i), Ti–O–Ti bridge stretching modes in regions (ii) and (iii) at 831 cm^{-1}, 806 cm^{-1}, 779 cm^{-1}, and 750 cm^{-1}, and a weak feature at 733 cm^{-1}. These calculated frequencies reproduce all features observed experimentally.

While structures **8-2**, **8-3**, **8-4**, and **8-5** can be considered degenerate with **8-1** within the accuracy of DFT, none of their simulated spectra can alone account for the features observed experimentally. Due to their higher levels of symmetry, they exhibit too few distinct IR active modes between 770 and 880 cm^{-1}. The same can be said for the energetically higher-lying isomers **8-8**, **8-9**, and **8-10**. It is possible that any of these structures could partially contribute to the congested structure we observe, but they cannot alone reproduce experimental features.

Isomers **8-6**, **8-7**, **8-11**, **8-12**, and **8-13**, on the other hand, are of C_1 symmetry with disordered geometries and demonstrate more IR activity between 770 and 880 cm^{-1}. Structure **8-12** can perhaps be ruled out as it has three terminal Ti–O bonds and therefore a relatively broad absorption in region (i), while the experimental feature in that region is quite narrow. The isomers **8-6**, **8-7**, **8-11**, and **8-13** cannot be ruled out from contributing to the spectrum but do not appear to match the overall spectral profile of the experimental results as well as isomer **8-1**.

We therefore assign the dominant contribution to the experimental spectrum to **8-1**, but cannot make a concrete statement about whether other isomers are also present. It is noteworthy that, like for $n = 5$, although there are many candidate $n = 8$ clusters, the IR spectrum for the lowest-lying DFT structure is a reasonable match to experiment and that many other low-lying structures can be easily ruled out.

Structural trends

The qualitative agreement between calculated and experimental IR spectra indicates that the candidate $(TiO_2)_n^-$ (n = 3-8) structures identified here and in the literature are reasonable. The experimental data we report are uniquely suited not only to identify the most likely cluster structures but also to highlight when the harmonic approximation does not capture the spectroscopic signatures of potentially fluxional clusters, as seen here for $n = 4$ and $n = 7$. However, the predicted global minimum energy DFT structures are satisfactory matches for many of the IRPD spectra reported here. It is possible that barriers between low-lying structures are small enough to facilitate population of the global minimum structure for each cluster size under the present experimental conditions. Using the best calculated structures for each $(TiO_2)_n^-$ cluster (**3-1**, **4-1**/**4-2**, **5-1**, **6-1**, **7-1**/**7-2**, and **8-1**), we can consider the size-dependent evolution of their properties.

The assigned clusters feature compact structures, with only two terminal Ti–O bonds and many bridging O atoms. Ti atoms have primarily 3- and 4-fold coordination, and O atoms, apart from the free Ti–O moieties, have primarily 2-fold coordination, occasionally 3-fold coordination (structures **3-1**, **7-1**, and **8-1**), and remarkably even 4-fold coordination (structure **6-1**). The level of coordination generally increases with cluster size. Structure **3-1** has an average Ti atom coordination of 3.67 and O coordination of 1.83 and **4-1** and **4-2** share an average Ti coordination of 3.50 and O coordination of 2.00; structures **6-1** and **8-1** meanwhile have respective Ti coordination numbers of 4.00 and 3.88, and O coordination numbers of 2.33 and 2.17. In both rutile and anatase bulk TiO_2, each Ti atom is coordinated with 6 O atoms in a roughly octahedral layout and each O atom has 3 Ti atoms coordinated in a trigonal planar geometry.[2] $(TiO_2)_n^-$ clusters do not reach this average level of coordination within the size range studied here.

In conjunction with lowered coordination relative to the bulk, the average Ti–O bond lengths in the small $(TiO_2)_n^-$ clusters are shorter than those of bulk TiO_2. Room temperature rutile and anatase TiO_2 have average Ti–O bond lengths of 1.96 Å.[77,78] The predicted bond lengths of the $(TiO_2)_n^-$ clusters stay fairly similar over the range of n studied here. The terminal Ti–O bonds are significantly shorter than those with higher coordination, falling consistently in the range of 1.64-1.66 Å for all n = 3-8 clusters. The average length of non-terminal Ti–O bonds ranges from 1.88 to 1.92 Å over n = 3-8, consistently shorter than the bulk values. Chen and Dixon[60] also report that both the coordination numbers and the average bond lengths of calculated neutral clusters as large as $n = 13$ fall short of the bulk values.

The IRPD spectra of the $(TiO_2)_n^-$ clusters also show some trends worth noting. All experimental spectra have IR absorption in region (i), due to the excitation of the terminal Ti–O stretching modes ubiquitous in the clusters studied here, though not present in bulk TiO_2. The frequencies of these Ti–O stretching features increase slightly with the size of the cluster, from as low as 948 cm^{-1} for $n = 3$ to as high as 989 cm^{-1} for $n = 8$. Additionally, the spacing between frequencies of the symmetric and antisymmetric terminal Ti–O stretching modes decreases with increasing cluster size. In n = 3-5, the experiment resolves a splitting in the region (i) features. For n = 6-8, no splittings are observed. The simulated spectra suggest that both symmetric and antisymmetric modes are IR active in these species but are too close in frequency to resolve in our experiment. The IR active modes in regions (ii) and (iii) also tend to shift towards higher frequency with larger cluster size. For n = 3-5, the highest frequency absorption in region (iii) increases from 746 cm^{-1} to 757 cm^{-1} to 781 cm^{-1}. Beginning with $n = 6$, the structural motif of three Ti–O–Ti bridges tetrahedrally coordinated to a terminal Ti–O moiety appears. This motif yields IR absorption in region (ii) and persists for larger n, with the highest frequency absorption in region (ii) at 854 cm^{-1} for $n = 6$, 851 cm^{-1} for $n = 7$, and 862 cm^{-1} for $n = 8$. The DFT calculated frequencies for the best predicted structures also follow these general trends (see the supplementary material);[81] with larger n, the strong features in regions (i)-(iii) shift towards higher frequencies and the splitting between the region (i) features decreases.

A final size-dependent property worth considering is the localization of the anion SOMO for the assigned $(TiO_2)_n^-$

clusters. The additional electron in the anion SOMO can perturb the cluster enough that the relative energies of specific isomers are drastically different for the anions and neutrals.[18] The SOMOs of relevant clusters are visualized in Fig. S1;[81] they are largely of $3d$ character localized on Ti atoms. As has been noted by Li and Dixon,[18] the **3-1** cluster anion SOMO is a $3d_z^2$ orbital localized entirely on the least-coordinated Ti atom, while the **4-1** and **4-2** clusters have SOMOs with $3d$ character distributed across two Ti atoms. Like the **3-1** cluster, the **5-1** cluster has a SOMO localized in a $3d_z^2$ orbital of a 3-fold coordinated Ti atom; the clusters with $n \geq 6$, however, have more delocalized SOMOs distributed over the $3d$ orbitals of four or more Ti atoms. In all species, the SOMO avoids localization on Ti atoms with terminal Ti–O bonds to reduce unfavorable repulsion of the excess electron density.

In bulk TiO_2, titanium centers are found as Ti^{4+} cations; oxygen vacancy defect sites on TiO_2 surfaces are therefore accompanied by under-coordinated Ti^{3+} cations. These Ti^{3+} centers are critical to reactive adsorption[3,79] and reduction of organic molecules[80] on TiO_2 surfaces. $(TiO_2)_n^-$ clusters with an excess electron localized on a single Ti atom, like those in the **3-1** and **5-1** structures, are similarly expected to be quite reactive. These clusters may, therefore, have strong reducing capability and may be reasonable analogs for Ti^{3+} defect sites on bulk TiO_2 catalytic surfaces. It would be of interest to see if these clusters are particularly reactive toward CO_2 and other electron-accepting species.

SUMMARY AND CONCLUSIONS

We report IRPD spectra for the messenger-tagged $(TiO_2)_n^-$ clusters with n = 3-8 in the 450-1200 cm^{-1} spectral range. DFT calculations are performed to determine the structures, energetics, and harmonic IR spectra of the most stable cluster isomers. Comparison of experimental and calculated spectra does not always allow clear identification of a single lowest energy cluster structure; however, the overall agreement between theory and experiment provides much new information about these species. We unambiguously assign the structures of $(TiO_2)_3^-$ and $(TiO_2)_6^-$, narrow down the contributions to the spectra for $(TiO_2)_4^-$ and $(TiO_2)_7^-$ to two isomers, and find that the $(TiO_2)_5^-$ and $(TiO_2)_8^-$ spectra satisfactorily match simulated spectra for the lowest energy isomer, even though these clusters have complex potential energy surfaces with many low-lying candidate structures.

The information reported here about the likely structures of small anionic titanium oxide clusters will be of great utility in guiding future spectroscopic work. In particular, applying the complementary technique of slow photoelectron velocity-map imaging[48] to these clusters could aid in distinguishing close-lying anion isomers that detach to neutrals more widely spaced in energy. Additionally, the $(TiO_2)_n^-$ clusters studied in this work have considerable potential as model systems for catalysis on bulk TiO_2. Of particular interest is the reduction of CO_2 on a TiO_2 surface; in forthcoming IRPD work, we aim to characterize the complexes formed after reaction of $(TiO_2)_n^-$ clusters with CO_2.

ACKNOWLEDGMENTS

This research is funded by the Air Force Office of Scientific Research under Grant No. FA9550-12-1-0160 and by the German Research Foundation (DFG) within the Collaborative Research Center 1109. M.L.W. thanks the National Science Foundation for a graduate research fellowship. X.S. thanks the Alexander von Humboldt foundation for a postdoctoral fellowship.

[1]N. N. Greenwood and A. Earnshaw, *Chemistry of the Elements*, 2nd ed. (Elsevier, Oxford, UK, 1998).
[2]U. Diebold, Surf. Sci. Rep. **48**, 53 (2003).
[3]T. L. Thompson and J. T. Yates, Chem. Rev. **106**, 4428 (2006).
[4]M. Anpo, S. Dohshi, M. Kitano, Y. Hu, M. Takeuchi, and M. Matsuoka, Annu. Rev. Mater. Res. **35**, 1 (2005).
[5]A. Fujishima and K. Honda, Nature **238**, 37 (1972).
[6]F. E. Osterloh, Chem. Mater. **20**, 35 (2008).
[7]Á. Valdés, Z.-W. Qu, G.-J. Kroes, J. Rossmeisl, and J. K. Nørskov, J. Phys. Chem. C **112**, 9872 (2008).
[8]M. Grätzel, Nature **414**, 338 (2001).
[9]A. J. Frank, N. Kopidakis, and J. van de Lagemaat, Coord. Chem. Rev. **248**, 1165 (2004).
[10]M. R. Hoffmann, S. T. Martin, W. Choi, and D. W. Bahnemann, Chem. Rev. **95**, 69 (1995).
[11]D. Bahnemann, Sol. Energy **77**, 445 (2004).
[12]H. He, P. Zapol, and L. A. Curtiss, J. Phys. Chem. C **114**, 21474 (2010).
[13]S. N. Habisreutinger, L. Schmidt-Mende, and J. K. Stolarczyk, Angew. Chem., Int. Ed. **52**, 7372 (2013).
[14]H. Zhang and J. F. Banfield, J. Mater. Chem. **8**, 2073 (1998).
[15]A. Bendavid, P. J. Martin, Å. Jamting, and H. Takikawa, Thin Solid Films **355**, 6 (1999).
[16]T. Tachikawa, M. Fujitsuka, and T. Majima, J. Phys. Chem. C **111**, 5259 (2007).
[17]S. A. Shevlin and S. M. Woodley, J. Phys. Chem. C **114**, 17333 (2010).
[18]S. Li and D. A. Dixon, J. Phys. Chem. A **112**, 6646 (2008).
[19]Z. R. R. Tian, J. A. Voigt, J. Liu, B. McKenzie, and H. Xu, J. Am. Chem. Soc. **125**, 12384 (2003).
[20]C. Ducati, E. Barborini, G. Bongiorno, S. Vinati, P. Milani, and P. A. Midgley, Appl. Phys. Lett. **87**, 201906 (2005).
[21]M. G. Manera, P. D. Cozzoli, M. L. Curri, G. Leo, R. Rella, A. Agostiano, and L. Vasanelli, Synth. Met. **148**, 25 (2005).
[22]G. K. Mor, K. Shankar, M. Paulose, O. K. Varghese, and C. A. Grimes, Nano Lett. **6**, 215 (2006).
[23]J. H. Park, S. Kim, and A. J. Bard, Nano Lett. **6**, 24 (2006).
[24]B. Liu and E. S. Aydil, J. Am. Chem. Soc. **131**, 3985 (2009).
[25]K. A. Zemski, D. R. Justes, and A. W. Castleman, J. Phys. Chem. B **106**, 6136 (2002).
[26]D. K. Böhme and H. Schwarz, Angew. Chem., Int. Ed. **44**, 2336 (2005).
[27]J. Sauer and H. J. Freund, Catal. Lett. **145**, 109 (2015).
[28]Y. Gong, M. Zhou, and L. Andrews, Chem. Rev. **109**, 6765 (2009).
[29]G. E. Johnson, R. Mitrić, V. Bonačić-Koutecký, and A. W. Castleman, Chem. Phys. Lett. **475**, 1 (2009).
[30]K. R. Asmis, Phys. Chem. Chem. Phys. **14**, 9270 (2012).
[31]Y. Matsuda and E. R. Bernstein, J. Phys. Chem. A **109**, 314 (2005).
[32]G. von Helden, D. van Heijnsbergen, and G. Meijer, J. Phys. Chem. A **107**, 1671 (2003).
[33]K. Demyk, D. van Heijnsbergen, G. von Helden, and G. Meijer, Astron. Astrophys. **420**, 547 (2004).
[34]E. Janssens, G. Santambrogio, M. Brümmer, L. Wöste, P. Lievens, J. Sauer, G. Meijer, and K. R. Asmis, Phys. Rev. Lett. **96**, 233401 (2006).
[35]B. Helmich, M. Sierka, J. Dobler, and J. Sauer, Phys. Chem. Chem. Phys. **16**, 8441 (2014).
[36]H. Wu and L.-S. Wang, J. Chem. Phys. **107**, 8221 (1997).
[37]H.-J. Zhai and L.-S. Wang, J. Am. Chem. Soc. **129**, 3022 (2007).
[38]G. V. Chertihin and L. Andrews, J. Am. Chem. Soc. **117**, 1595 (1995).
[39]K. M. Perera and R. B. Metz, J. Phys. Chem. A **113**, 6253 (2009).
[40]E. C. Tyo, M. Nößler, R. Mitrić, V. Bonačić-Koutecký, and A. W. Castleman, Phys. Chem. Chem. Phys. **13**, 4243 (2011).
[41]J. Zhuang, Z. H. Li, K. Fan, and M. Zhou, J. Phys. Chem. A **116**, 3388 (2012).
[42]S. Yin and E. R. Bernstein, Phys. Chem. Chem. Phys. **16**, 13900 (2014).
[43]G. V. Chertihin and L. Andrews, J. Phys. Chem. **99**, 6356 (1995).

[44]S. Brünken, H. S. P. Müller, K. M. Menten, M. C. McCarthy, and P. Thaddeus, Astrophys. J. **676**, 1367 (2008).
[45]X. J. Zhuang, A. Le, T. C. Steimle, R. Nagarajan, V. Gupta, and J. P. Maier, Phys. Chem. Chem. Phys. **12**, 15018 (2010).
[46]J. B. Kim, M. L. Weichman, and D. M. Neumark, Phys. Chem. Chem. Phys. **15**, 20973 (2013).
[47]Y. Gong, Q. Zhang, and M. Zhou, J. Phys. Chem. A **111**, 3534 (2007).
[48]J. B. Kim, M. L. Weichman, and D. M. Neumark, J. Am. Chem. Soc. **136**, 7159 (2014).
[49]T. Albaret, F. Finocchi, and C. Noguera, J. Chem. Phys. **113**, 2238 (2000).
[50]S. Hamad, C. R. A. Catlow, S. M. Woodley, S. Lago, and J. A. Mejías, J. Phys. Chem. B **109**, 15741 (2005).
[51]Z. W. Qu and G. J. Kroes, J. Phys. Chem. B **110**, 8998 (2006).
[52]S. M. Woodley, S. Hamad, J. A. Mejías, and C. R. A. Catlow, J. Mater. Chem. **16**, 1927 (2006).
[53]M. Calatayud, L. Maldonado, and C. Minot, J. Phys. Chem. C **112**, 16087 (2008).
[54]M.-H. Weng, C. Chen, and S.-P. Ju, Chin. J. Catal. **30**, 384 (2009).
[55]I. Bandyopadhyay and C. M. Aikens, J. Phys. Chem. A **115**, 868 (2011).
[56]O. A. Syzgantseva, P. Gonzalez-Navarrete, M. Calatayud, S. Bromley, and C. Minot, J. Phys. Chem. C **115**, 15890 (2011).
[57]W. Zhang, Y. Han, S. Yao, and H. Sun, Mater. Chem. Phys. **130**, 196 (2011).
[58]L. L. Tang, L. W. Sai, J. J. Zhao, and R. F. Qiu, J. Comput. Chem. **33**, 163 (2012).
[59]N. Marom, M. Kim, and J. R. Chelikowsky, Phys. Rev. Lett. **108**, 106801 (2012).
[60]M. Y. Chen and D. A. Dixon, J. Chem. Theory Comput. **9**, 3189 (2013).
[61]S. Ganguly Neogi and P. Chaudhury, J. Comput. Chem. **35**, 51 (2014).
[62]S. G. Li and D. A. Dixon, J. Phys. Chem. A **114**, 2665 (2010).
[63]K. R. Asmis, M. Brümmer, C. Kaposta, G. Santambrogio, G. von Helden, G. Meijer, K. Rademann, and L. Wöste, Phys. Chem. Chem. Phys. **4**, 1101 (2002).
[64]T. R. Rizzo, J. A. Stearns, and O. V. Boyarkin, Int. Rev. Phys. Chem. **28**, 481 (2009).
[65]A. B. Wolk, C. M. Leavitt, E. Garand, and M. A. Johnson, Acc. Chem. Res. **47**, 202 (2014).
[66]K. R. Asmis and J. Sauer, Mass Spectrom. Rev. **26**, 542 (2007).
[67]M. Brümmer, C. Kaposta, G. Santambrogio, and K. R. Asmis, J. Chem. Phys. **119**, 12700 (2003).
[68]D. J. Goebbert, G. Meijer, and K. R. Asmis, AIP Conf. Proc. **1104**, 22 (2009).
[69]D. J. Goebbert, T. Wende, R. Bergmann, G. Meijer, and K. R. Asmis, J. Phys. Chem. A **113**, 5874 (2009).
[70]W. Schöllkopf, S. Gewinner, H. Junkes, A. Paarmann, G. von Helden, H. Bluem, and A. M. M. Todd, Proc. SPIE **9512**, 95121L (2015).
[71]T. M. Maier, A. D. Boese, J. Sauer, T. Wende, M. Fagiani, and K. R. Asmis, J. Chem. Phys. **140**, 204315 (2014).
[72]S. G. Li and D. A. Dixon, J. Phys. Chem. A **111**, 11908 (2007).
[73]A. J. Wachters, J. Chem. Phys. **52**, 1033 (1970).
[74]P. J. Hay, J. Chem. Phys. **66**, 4377 (1977).
[75]S. Grimme, J. Comput. Chem. **27**, 1787 (2006).
[76]M. J. Frisch, G. W. Trucks, H. B. Schlegel, G. E. Scuseria, M. A. Robb, J. R. Cheeseman, G. Scalmani, V. Barone, B. Mennucci, G. A. Petersson, H. Nakatsuji, M. Caricato, X. Li, H. P. Hratchian, A. F. Izmaylov, J. Bloino, G. Zheng, J. L. Sonnenberg, M. Hada, M. Ehara, K. Toyota, R. Fukuda, J. Hasegawa, M. Ishida, T. Nakajima, Y. Honda, O. Kitao, H. Nakai, T. Vreven, J. A. Montgomery, J. E. Peralta, F. Ogliaro, M. Bearpark, J. J. Heyd, E. Brothers, K. N. Kudin, V. N. Staroverov, R. Kobayashi, J. Normand, K. Raghavachari, A. Rendell, J. C. Burant, S. S. Iyengar, J. Tomasi, M. Cossi, N. Rega, J. M. Millam, M. Klene, J. E. Knox, J. B. Cross, V. Bakken, C. Adamo, J. Jaramillo, R. Gomperts, R. E. Stratmann, O. Yazyev, A. J. Austin, R. Cammi, C. Pomelli, J. W. Ochterski, R. L. Martin, K. Morokuma, V. G. Zakrzewski, G. A. Voth, P. Salvador, J. J. Dannenberg, S. Dapprich, A. D. Daniels, Ö. Farkas, J. B. Foresman, J. V. Ortiz, J. Cioslowski, and D. J. Fox, GAUSSIAN 09, Revision C.01, Gaussian, Inc., Pittsburgh, PA, 2009, http://www.gaussian.com.
[77]E. P. Meagher and G. A. Lager, Can. Mineral. **17**, 77 (1979).
[78]M. Horn, C. F. Schwerdtfeger, and E. P. Meagher, Z. Kristallogr. **136**, 273 (1972).
[79]W. S. Epling, C. H. F. Peden, M. A. Henderson, and U. Diebold, Surf. Sci. **412-413**, 333 (1998).
[80]G. Lu, A. Linsebigler, and J. T. Yates, J. Phys. Chem. **98**, 11733 (1994).
[81]See supplementary material at http://dx.doi.org/10.1063/1.4942194 for details of calculated $(TiO_2)_n^-$ isomer electronic states, energetics, geometries, and vibrational frequencies, visualizations of singly occupied molecular orbitals, and additional simulated IR spectra.